JAERI-M
9780

ONE-DIMENSIONAL SYSTEM ANALYSIS CODE FOR REFLOOD PHASE DURING LOCA

November 1981

Yoshio MURAO and Jun SUGIMOTO

日本原子力研究所
Japan Atomic Energy Research Institute

JAERI-M 9780

One-dimensional System Analysis Code for Reflood Phase during LOCA

Yoshio MURAO and Jun SUGIMOTO

Division of Reactor Safety,

Tokai Research Establishment, JAERI

(Received October 14, 1981)

A system code named REFLA-1D was developed by coupling the core thermo-hydrodynamic code and the primary system model for the analysis of the reflood phenomena.

In order to assess the calculation method of this system code, the results of a base case test and parametric tests, which were run for the conditions of the base case test by varying only one parameter at a time, were compared with the results calculated with the system code.

The calculation of the base case test showed a good agreement with the data for the core collapsed liquid level, the quench front elevation, and the heat transfer coefficient near the quench front.

The calculation of the parametric test showed a good agreement with the data for the effect of the initial clad temperature and of the peak power, however, a good agreement was not obtained for the effect of system pressure.

Further study of the two-phase flow modeling in the core and the quench front correlation against the pressure dependence is necessary for a better prediction of the system behaviors.

Keywords: PWR, LOCA, Reflood, Computer Code, Quenching, Thermo-hydrodynamics, Heat Transfer, Two-phase Flow

JAERI－M 9780

LOCA時再冠水過程一次元システム解析コード

日本原子力研究所東海研究所安全工学部
村尾良夫・杉本　純

（1981年10月14日受理）

再冠水現象解析のため，炉心熱水力コードと一次系システムモデルを結合したシステムコードREFLA－1Dを開発した。

本システムコードの計算手法の評価のため，原研の再冠水実験の中の基準実験，パラメータ効果実験の結果を本システムコードの計算と比較した。

基準実験の解析では，炉心液位，クエンチ点の進行，クエンチ点近傍の熱伝達率について計算値と実験データとの良い一致が得られた。

パラメータ効果実験の解析では，初期発熱棒温度および発熱棒出力の効果については実験データとの良い一致が得られたが，系圧力の効果については良い一致が得られなかった。

システム挙動のより精度の高い予測のためには，炉心内二相流モデルやクエンチ相関式の圧力依存性についての検討が必要である。

Contents

List of tables

List of figures

I. Introduction

In nuclear reactor safety, much of the current interest has been paid in the reflood phenomena. In a loss of coolant accident (LOCA), the reactor core may be uncovered, resulting in a temperature excursion of the fuel cladding. To prevent disintegrity of the cladding due to overheating, the emergency core cooling system (ECCS) is provided to reflood the core with water. The temperature excursion of the cladding is then limited by the efficacy of the reflood processes. In the safety analysis in the LOCA, it is very important to evaluate the temperature history of the fuel claddings during the reflood phase, which governs the integrity of the first enclosure of the fission product. Fig. 1(a) illustrates a possible temperature-time history at the midplane of the core during reflood phase. The time of the termination of the temperature excursion is called the turn-around time. The time when the temperature falls down rapidly is called the quench time.

In order to investigate the thermo-hydrodynamic behavior, many flooding experiments were conducted. The most important experiments were in the PWR-FLECHT program and its continuation, the FLECHT-SET program. These programs generated heat transfer correlations and fluid flow data used for the licensing of PWRs. Based on the data, it was found that the heat transfer coefficient increased significantly and the quench time decreased with increased flooding rate (core inlet flow rate) which caused an increased vapor generation rate and liquid entrainment. The flooding rate is controlled by the balance between the driving head which forces the water into the core (the head of water in

the downcomer minus that in the core), and the back pressure in the upper plenum created by the steam-water mixture flowing from the core exit to the break. The downcomer head has a maximum value because water exceeding the level of a broken cold leg nozzle will spill over. The back-pressure effect, which opposes the core flooding with water during reflood phase, is called "Steam binding". Therefore the core thermo-hydrodynamics is strongly linked with the system thermo-hydrodynamics.

In the safety evaluation of the reflood phase of PWR, the empirical correlations being given by numerical data on the reflood heat transfer and the carryover rate fraction were used. The latter is used for calculating the conditions of the core inlet. This method is valid for the quasi-steady-state analysis without extrapolation outside the experimental range. For flexibility in the application to safety analysis, a best-estimate computer code of the reflood process based on the physical understanding of the phenomena was determined to be developed.

As a first stage, we developed a one-dimensional core thermo-hydrodynamic code named REFLA-1D[1),(2)] for a single coolant channel in a reactor core with bottom coolant injection at a constant flow rate. This is the basis for the extension to an integral reflood analysis code.

This code fairly good results[3)]. As shown in Fig. 2, the heat transfer coefficient of midplane calculated with $W_{ec} = 1$ agreed with those of PWR-FLECHT except those in low flooding cases ($u_{\ell in} < 2.5$ cm/sec) and those in the transition flow region (identified as flat parts in calculated results and called as inverted annular flow regions.)

In the FLECHT-SET Phase-A system effect experiments[4], the oscillations of the downcomer and bundle water levels and flooding rate were observed. The periods nearly agreed with the periods of U-tube type oscillation of the water in the downcomer, the core and the pipe connecting them. In similar experiments conducted at JAERI it was concluded that this oscillation was excited by the oscilation of the back-pressure which was measured from the phase difference between the oscillation of flooding rete and back-pressure[5].

The objective of the present study is the establishment of the system analysis model based on the dynamic behavior. The one-dimensional system analysis code (named REFLA-1D system code) was developed coupling the modified REFLA-1D core model with the system model and compared with measured data for evaluation of the code.

Ⅱ. Mathematical expression of reflood model

1. Core model

1.1 Flow pattern

The following two reflood flow madels were assumed as shown in Fig.3 depending on different flow pattern.

(1) Type 1 flow pattern is characterized by subcooled condition at the bottom quench front. In the upstream of the bottom quench front, the injected water flows the liquid phase region and the subcooled nucleate boiling region. In the downstream of the bottom quench front, the water flows the subcooled film boiling region (the water temperature is lower than the saturation temperature), the transition flow region (the water is at the saturation temperature and the criterion for transition is not satisfied), the dispersed flow region (the transition criterion is satisfied and droplets are entrained and accelerated), and the rewetted region (or the wall temperature is lower than a critical temperature) or the superheated steam flow region (only when water does not exist in the region downstream of the top quench front).

(2) Type 2 flow pattern, on the other hand, shows saturated conditions at the bottom quench front. The flow pattern is nearly the same as the Type 1 except for the regions near the bottom quench front. The saturated two-phase flow region appears upstream from the bottom quench front and a subcooled film boiling region does not appear downstream from the the quench front.

The definition of the boundaries and the boundary conditions of each region is also described in Fig.3. The boundary just

below the dispersed flow is called the froth level.

1.2 Basic thermo-hydrodynamic equations for coolant

Based on the assumption of perfectly separated one-dimensional two-phase flow, the Eulerian equations for the conservation of mass, momentum and energy for two-phase fluid flowing upward in a vertical channel are:

Continuity for the vapor phase

$$\frac{\partial(\alpha\,\rho_g)}{\partial t} + \frac{\partial(\alpha\rho_g U_g)}{\partial Z} = \dot{m} \tag{1}$$

Continuity for the liquid phase

$$\frac{\partial\{(1-\alpha)\rho_\ell\}}{\partial t} + \frac{\partial\{(1-\alpha)\rho_\ell U_\ell\}}{\partial Z} = -\dot{m} \tag{2}$$

Momentum for the vapor phase

$$\frac{\partial(\alpha\rho_g U_g)}{\partial t} + \frac{\partial(\alpha\rho_g U_g^2)}{\partial Z} + \alpha\frac{\partial p}{\partial Z} + \alpha\rho_g\, g + V_g = \dot{m}U_\ell \tag{3}$$

Momentum for the liquid phase

$$\frac{\partial\{(1-\alpha)\rho_\ell U_\ell\}}{\partial t} + \frac{\partial\{(1-\alpha)\ell_\ell U_\ell^2\}}{\partial Z} + (1-\alpha)\frac{\partial p}{\partial Z}$$

$$+ (1-\alpha)\rho_\ell g + V_\ell = -\dot{m}U_\ell \tag{4}$$

Energy for the vapor phase

$$\frac{\partial(\alpha\rho_g g\, H_g)}{\partial t} + \frac{\partial(\alpha\rho_g g\, U_g H_g)}{\partial Z} = Q_g + \dot{m}gH_g \tag{5}$$

Enerty for the liquid phase

$$\frac{\partial\{(1-\alpha)\rho_\ell g\ H_\ell\}}{\partial t} + \frac{\partial\{(1-\alpha)\rho_\ell g\ U_\ell H_\ell\}}{\partial Z} = Q_\ell - \dot{m}gH_g \qquad (6)$$

1.3 Generalized equations for the core

It was assumed that:

(1) The two-phases are perfectly separated.

(2) The physical properties of the liquid are function of only the ststem pressure and liquid of two-phase mixture has saturation temperature.

(3) The physical properties of the vapor are functions of the system pressure and the vapor tmperature. The specific heat of the vapor is constant and the vapor is considered as an idela gas, i.e.

$$H_g = H_{sat} + H_{fg} + C_{pg}\ (T_g - T_{sat}) \qquad (7)$$

$$P_g = P_{gsat}\ (T_{sat} + 273.16)/(T_g + 273.16) \qquad (8)$$

(4) Core inlet pressure is represented by system pressure.

Under the above assumption, Eqs. (1) to (6) can be rewritten in the following forms:

(Adding Eqs. (1) and (2))

$$\partial\{\alpha\rho_g + (1-\alpha)\rho_\ell\}/\partial t + \partial G/\partial Z = 0\ , \qquad (9)$$

(Eq.(5) -Eq.(1) × $H_g g$ and arranging with Eq.(7))

$$\partial T_g/\partial t + U_g\ \partial T_g/\partial Z = Q_g/(\alpha\rho_g C_{pg} g)\ , \qquad (10)$$

(Eq.(6) - Eq.(2) multiplied by $H_\ell\ g$ and arranging)

$$\dot{m} = Q_\ell / \{H_{fg}g + C_{pg}g\ (T_g - T_{sat})\} \ , \tag{11}$$

((Eq.(5) + Eq.(6)) - (Eq.(1) + Eq.(2)) × H_ℓ g and arranging)

$$\partial(\alpha\rho_g)/\partial t + \partial G_g/\partial Z = \dot{m} \ , \tag{12}$$

(Eq.(3) + Eq.(4))

$$\partial G/\partial t + (1/\rho_\ell)\partial D_v/\partial Z + \partial p/\partial Z + g\{\alpha\rho_g + (1-\alpha)\rho_\ell\} + V_\ell + V_g = 0 \ , \tag{13}$$

where $G_g = \rho_g U_g \alpha$, (14)

$$G = G_g + \rho_\ell U_\ell (1-\alpha) \ , \tag{15}$$

and $D_v = \{\rho_\ell/(\alpha\rho_g)\}G_g^2 + 1/(1-\alpha)\}(G-G_g)^2$. (16)

One additional momentum euqation is necessary to be equivalent to the set of original equations. Instead of the additional momentum equation, a correlation for slip velocity ΔU is defined as $U_g - U_\ell$ and if G and G_g are given, the void fraction can be derived, i.e.

$$\alpha = \frac{1}{2}\left(1 + \frac{C1 + C2}{\Delta U} - \sqrt{1 + \frac{2(C2 - C1)}{\Delta U} + \left(\frac{C1 + C2}{\Delta U}\right)^2}\right) \ , \tag{17}$$

where $C1 = G_g/\rho_g$, (18)

and $C2 = (G - G_g)/\rho_\ell$. (19)

In single liquid phase flow, Eqs. (10) and (11) are replaced as follows:

$$\partial T_\ell/\partial t + \partial(U_\ell T_\ell)/\partial Z = Q_\ell/(\rho_\ell D_{p\ell} g) \quad , \tag{20}$$

and $\dot{m} = 0$. (20)'

1.4 Thermo-hydrodynamic correlations used in core model

(1) Liquid phase flow region

Single liquid phase flow is used for the hydrodynamic model and saturated nucleate boiling is assumed for the heat transfer model. Even in the non-boiling region, a saturated nucleate boiling heat transfer model is used for the calculation of the clad temperature.

(2) Saturated two-phase flow region

Thermal equilibrium is assumed between the two phases Cunningham-Yeh's correlation[6] is adopted for the void fraction correlation which is used to calculate the slip velocity, ΔU; that is,

$$\Delta U = G_g/(\alpha_{yen} \cdot \rho_g) \quad . \tag{21}$$

Frictional pressure loss is neglected. Saturated nucleate boiling is assumed for the heat transfer model.

(3) Transition flow region

Because of lack of information for this region, the same model described in (2) above is adopted for the hydrodynamic model. For the heat transfer coefficent,

$$h_{sat} = 0.94(1-\alpha)^{0.25}\{\lambda_g^{\,3}\ \rho_g(\rho_\ell - \rho_g)\cdot H_{fg}\cdot g / (L_Q \mu_g)(T_w - T_{sat})\}^{0.25} \tag{22}$$

$$h_R = E(1-\alpha)^{0.5}\ \varepsilon(T_w^{\,4} - T_{est}^{\,4})/(T_w - T_{sat}) \quad . \tag{23}$$

The above correlations were developed by Murao and Sugimoto[7],[8].

(4) Subcooled film boiling region

According to many researchers, the parameter of the liquid subcooling is thought to be most sensitive parameter and Kalinin[9] developed the correlation of a multiplication for the saturated film boiling with his data of liquid-nitrogen experiments. But for water, Kalinin's correlation was found to be invalid. Sudo[10] developed a multiplication factor of the saturated film boiling for subcooled film boiling based on his data and PWR-FLECHT data[11]. The multiplication factor F ($\equiv h_{sub}/h_{sat}$) is written as:

$$F = 1.0 + 0.025 \cdot (T_{sat} - T_{\ell}) \quad . \tag{24}$$

The basic hydrodynamic equations in the single liquid flow region without frictional pressure loss is applied for subcooled film boiling region because the thin vapor film was considered a lubricant.

(5) Dispersed flow region

It was assumed that:

1) So called two step model is available; that is, the heat is transferred from the heated wall to the vapor and from the vapor to the droplets by convection heat transfer and from the heated wall to the droplets by radiation heat transfer.
2) Spherical droplet configuration is considered for calculation of the viscous force and the heat transfer.
3) Slip velocity $\Delta U \equiv (U_g - U_{\ell})$ is equal to the free fall velocity of a droplet; in other words, the gravity

force balances with the drag force, i.e.

$$(1-\alpha)\rho_\ell g = V_\ell \quad . \tag{25}$$

4) Diameter of a droplet is calculated by the following correlation of the critical Weber number:

$$W_{ec} = \rho_g \, \Delta U_{crit}^2 \, D_d/\sigma \quad . \tag{26}$$

The Weber number is a dimensionless parameter of the ratio of the kinetic energy of the fluid around the droplet to the surface energy of the droplet. It is throught to have a maximum value; that is, if the kinetic energy of the droplet and the surface energy increases to a limiting value, the droplet becomes unstable and bursts. Though critical Weber number, We_c, recommended by Groeneveld is 6.5[12], We_c could not be fixed because of a lack of data.

5) For the drag coefficient of spherical droplets, the Ingebo's correlation[13] is adopted, i.e.

$$C_D = 27 \, R_e^{-0.84} \tag{27}$$

and $C_{Dmin} = 0.4$

From the assumption of spherical droplets, the following relations are derived:

$$V_\ell = - \frac{n}{U_\ell} C_D \frac{1}{2} \rho_g \Delta U^2 \cdot \pi \frac{D_d^2}{4} \quad , \tag{28}$$

$$\frac{n}{U_\ell} = (1-\alpha) / \{\frac{4}{3} \pi (\frac{D_d}{2})^3\} \quad . \tag{29}$$

Arranging Eqs. (24) to (29), the following critical

slip velocity ΔU_{crit} is obtained:

$$\Delta U_{crit} = \min (\Delta U_2 , \Delta U_3) \quad , \tag{30}$$

were

$$\Delta U_2 = 0.53713 \cdot (\rho \cdot We_c)^{0.3802} \cdot \rho_g^{-0.5868} \cdot \nu^{-0.1736} \cdot (\rho_\ell \cdot g)^{0.2066} \quad , \tag{31}$$

$$\Delta U_3 = 1.3512 \left(\frac{\rho_\ell \cdot g \ We_c}{\rho_g^2} \right)^{0.25} \quad , \tag{32}$$

(from $C_D = 0.4$)

and min(a,b) indicates the minimum of the values a and b. The droplet size can be calculated as,

$$D_d = \frac{We_c \cdot \sigma}{\rho_g \cdot \Delta U^2_{crit}} \quad . \tag{33}$$

(6) Superheated steam flow

Single phase gas model is used in thermo-hydrodynamic model.

(7) Rewetted region

Top quench is not considered because it was found that the present quench model does not apply to top quench and a minor effect of top quenching on the over-all thermo-hydrodynamic behavior was observed.

1.5 Determination of boundaries of flow patterns.

(1) Determination of liquid top

In order to determine the liquid top, the rest of water above the current calculational node in the core is monitored.

The water remaining from the previous time t was stored and added to the water entering the core during Δt. The total amount of water indicates the available water during Δt. The water consumed below the calculational node is subtracted from the total and the rest of the water, which is the available water above the calculational node, is monitored. When the water above the calculational node does not exist, the liquid top is interpolated. This procedure is also valid for reverse flow.

(2) Quench front propagation

Murao's correlation[14] is adopted for the propagation of the bottom quench front. The correlation is written as

$$U_Q^{-1} = C_p \rho_g (T_Q - T_o)/\{2.19 \times 10^6 \ (\mathrm{kcal/m^2h}) \tag{34}$$

$$\times (1 + 0.2778 \times 10^{-4} \Delta T_{sub}^3)\} \tag{34}$$

where $T_o = 321.05 + 0.237 \times 10^{-4} p(\mathrm{kg/m^2})$ (35)

$C_p \rho_g$ of the clad material is assumed to be 927.48 (kcal/m^3°C) in the code. This value is valid for stainless steel.

(3) Froth level

Froth level is interporated from ΔU_{j+1} and ΔU_j, when ΔU_{j+1} exceeds ΔU_{crit}. ΔU_{j+1} is calculated with Eq. (21) and ΔU_{crit} is calculated with Eq. (30).

1.6 Summary of the thermo-hydrodynamic correlation used in each flow region and the governing equations for the core

Correlations used in this model are listed in Table 1 and governing equations for the core are listed in Table 2.

1.7 Thermal equations in the fuel rod

To simplify the calculation, it was assumed that:

(1) The radial temperature profile is uniform; that is, the one point model can be adopted for the temperature calculation of the fuel rod and the axial heat conduction is negligible.

(2) In the quenched region, because of a small change of the fuel temperature with time, the heat transferred from the fuel to the coolant is nearly the same as the heat generated in the fuel rod.

(3) As ilustrated in Fig.1(b), the clad temperature rapidly decreases from T_Q to a quasi-steady-state temperature.

Therefore, in the quenched region, the wall temperature can be calculated without consideration of the stored energy release, i.e.,

$$S_F Q_F = SQ \ , \tag{36}$$

where Q is the heat transfer rate per unit volume of the coolant channel and a function of the wall temperature and the coolant temperature, i.e.,

$$Q = f(T_W , T_\ell) \ . \tag{37}$$

The thermal equation of the fuel rod can be written as,

$$S_F C_F \rho_F g \partial T_W / \partial t = S_F Q_F - SQ \ . \tag{38}$$

In the unquenched region, the wall temperature T_W is calculated from Eq. (38) by setting the heat transfer rate $Q = Q_g + Q_\ell$ in the dispersed flow region. In the quenched region, Q is calculated from Eq. (38) by first calculating T_W from Eq. (37). In the quenching region, as

illustrated in Fig.4, the additional heat Q'; which is a fraction, A_{st}, of the total stored energy indicated by hatched region, and is released at the quench front and transferred to unit area of coolant channel; can be obtained as follows:

$$AQ' = A_{st}\ S_F C_F \rho_F g\ (T_Q - T_W) U_Q \ . \tag{39}$$

It is assumed that when the quench front enters the i-th node, $(1 - A_{st})$ fraction of total stored energy of the i-th node starts to be release at time constant τ.

2. System model

In a PWR LOCA, the water-steam mixture is considered to flow in primary loops and the water part of the mixture is vaporized in the steam generators. Then the all mixture flows through the pumps which is estimated to be main pressure drop in the loop. Therefore, the steam flow seems to be dominant in the primary loops between the hot leg and ECC injection ports of the cold leg. On the other hand, the injected water seems to accumulate in the bottom of the reactor vessel; that is, the lower part of the downcomer, the core and the lower plenum. Because of the low mass velocity of injected water, the frictional pressure head is negligible as compared with the gravitational pressure head in the downcomer and the core. Therefore, the motion of the water accumulated in the bottom of reactor vessel can be treated as the motion of a single phase liquid of collapsed water in this region.

It was assumed that (1) the motion of water in the bottom of a reactor vessel is one-dimentional, (2) the water forms a

U-tube filled with a single phase liquid, and (3) both ends of the U-tube are connected with the primary loops where the single phase steam is flowing.

Our main objectives were to examine the possibility of stable and reasonable calculation with the above-mentioned model. Therefore, a simplified system model was introduced; that is, the entrained water from the core is completely separated and removed from the system, and only steam from the core enters in a single loop with an orifice as a flow resistance. The core and the downcomer are thought to be one-dimensional in the model. The schematic diagram of the model is similar to the system of FLECHT-SET A and is shown in Fig.5.

2.1 Basic equations and derivation of the final forms

Conservation equations of mass in the downcomer and the core are:

$$G_O - A_D \rho_\ell \dot{x} = A_I \rho_\ell U_I \quad , \tag{40}$$

$$\text{and} \quad A_I \rho_\ell U_I = A_C (\rho_\ell \dot{y} + G_{g\ out} + G_{\ell\ out}) \quad , \tag{41}$$

where G_O is the injection mass flow rate into the system and $G_{g\ out}$ and $G_{\ell\ out}$ are the steam and liquid mass flow rate at the exit of the core, respectively.

Conservation equations of momentum in the primary loop, the downcomer, the lower plenum (or downcomer-core connecting pipe) and the core are

$$P_U - P_S = K_L\ (\rho_g/2)\ U_L^2 \quad , \tag{42}$$

$$\rho_\ell \frac{d}{dt} (x\dot{x}) = P_D - P_S - \rho_\ell g x - K_D (\rho_\ell/2) |\dot{x}| \dot{x} \quad , \tag{43}$$

$$\rho_\ell \frac{d}{dt} (L_I U_I) = P_D - P_I - K_I(\rho_\ell/2)|U_I|U_I \quad , \tag{44}$$

and $$\rho_\ell \frac{d}{dt} (y\dot{y}) = P_I - P_U - \rho_\ell g y - K_C(\rho_\ell/2)|U_I|U_I \quad , \tag{45}$$

where $$U_C = \frac{A_I}{A_C} U_I \quad , \tag{46}$$

and $$X \leq X \max \ . \tag{46'}$$

$$V_U \frac{d P_U}{dt} = R\, T_U (A_C\, G_{g\ out} - A_L\, \rho_g\, U_L) \quad , \tag{47}$$

where V_U and T_U are the volume and the absolute temperature of the upper plenum respectively, R is a gas constant of ideal gas and T_U is assumed to be the saturation temperature.

Arranging the above equations, the following equations are derived:

$$U_I = (G_o - A_D\, \rho_\ell\, \dot{x})/(A_I\, \rho_\ell) \quad , \tag{48}$$

$$YD = - \frac{A_D}{A_C} x + \frac{G_o}{A_C\, \rho_\ell} - \frac{G_{\ell\ out} + G_{g\ out}}{A_C\, \rho_\ell} \quad , \tag{49}$$

$$U_C = \frac{A_I}{A_C} U_I \quad , \tag{50}$$

$$\begin{aligned} \ddot{x} = \{ & (P_U - P_S/\rho_\ell + (y - x)g + YD^2 - \dot{x}^2 \\ & + \frac{1}{2} (K_I|U_I|U_I + K_C|U_C|U_C - K_D|\dot{x}|\dot{x}) \\ & + \frac{1}{g\, \rho_\ell} \{ (\frac{L}{A_I} + \frac{y}{A_C}) \frac{d}{dt} G_o - \frac{y}{A_C} \frac{d}{dt} (G_{g\ out} + G_{\ell\ out}) \} \\ & / (x + y \frac{A_D}{A_C} + L \frac{A_D}{A_I}) \end{aligned} \quad , \tag{51}$$

$$\dot{y} = yD \quad , \tag{52}$$

$$\text{and} \quad \dot{P}_U = [\, RT_U \{A_C G_{g\ out} - A_L \frac{2\rho_g}{K_L} \cdot (P_U - P_S)\}]/V_U . \qquad (53)$$

Defining y_1, y_2, y_3 and y_4 as follows:

$$y_1 \equiv x, \quad y_2 \equiv \dot{x}, \quad y_3 \equiv P_U \text{ and } y_4 \equiv y \ ,$$

the above equations (48) to (58) can be written in following form, e.,

$$\frac{d}{dt} y_i = F_i(y_1, y_2, y_3, y_4) \ , \quad (i = 1 \sim 4) \ . \qquad (54)$$

2.2 Coupling the core model with the system model

When G_o and a set of variables $Y \equiv (G_{g\ out}, G_{\ell\ out})$ are given, a set of unknown nariables $X \equiv (x, y, U_I, P_D, P_I, P_U)$ can be solved by Eq.(54).

The REFLA-1D core code can calculate a set of variables Y, when the core inlet water temperature T_I, flooding rate U_I and pressure P_I are given. U_I and P_I are variables in X. In the REFLA-1D core code, physical properties refer to the core inlet pressure P_I. Therefore calculations can proceed as shown in Fig.6. In the system model, the Runge-Kutta-Gill method is used to solve the simultaneous equations (54). As the time step increment required for the system calculation is generally smaller than that of the core calculation, the same value of Y is used in each time step increment of the core calculation in solving in Eq.(54).

III. Test facility and test porcedure

To evaluate the dynamic and static characteristics of the REFLA-1D system code, selected data from small scale reflood experiments carried out in Japan Atomic Energy Research Institute (JAERI)[15] were compared with calculated results of the code. JAERI's small scale reflood test facility is analogous in system to the model considered for the present code as shown in Fig.5. This facility is similar to FLECHT-SET Phase-A facility[4] and has a core flow area scaled to 1/2100 of 1000 MWe class PWR. It can be operated in a gravity feed mode and a forced feed mode for the injection of water into the core.

The small scale reflood test facility consisted of a simulated 4 × 4 core with full length electrically heated rods, simulated upper and lower plenums, a simulated downcomer separated from a core flow channel, a simulated primary loop with equivalent flow resistance, and a simulated containment vessel.

In the test section, sixteen full length, electrically heated rods with Inconell-600 claddings were mounted in egg-crate type grid spacers of square lattice. A chopped-cosine axial power and a flat radial power profile were used. The nominal peaking factor was 1.6. The total power was kept constant during the transient without simulating reactor decay heat. The heated rods were designed for a maximum temperature of 1200°C using boron nitride insulation. Downcomer was made of unheated pipe with an over-flow nozzle for simulating a broken cold leg nozzle. The downcomer and the core form an one-dimentional U-tube and a water separator was built in the upper plenum. The separated water was drained into a tank to

measure the entrainment rate and steam was introduced into the loop. In the loop, an orifice was installed to provide flow resistance which is representative of the flow resistance of PWR primary loops and to measure steam flow rate.

The major specifications of the test facility are listed Table 3.

Instrumentation for tests included thermocouples embedded in grooves on the outside surface of the heater-rod cladding (at the 0.325, 0.8, 1.3, 1.5, 1.8, 2.1, 2.3, 2.55, 2.9 and 3.275-m elevations), fluid thermocouples, drag disk and turbine flow meters, differential pressure transducers, and pressure transducers. The signals from the detectors were recorded on a digital magnetic tape for the data reduction by the central computer.

The experiments were conducted as follows: The rod bundle and its housing were preheated to the predetermined initial temperature and then the reflooding was initiated by injecting the water into the downcomer.

The relevant parameter ranges referred to are listed in Table 4. These tests were run for the base case conditions by varying only one parameter at a time. The base case conditions are listed in Table 5.

IV. Results and Discussion

1. Estimation of the core inlet flow resistance of the JAERI small scale reflood experiment

The flow area of the connecting pipe between the core and the downcomer was about 1/4 times smaller than the flow area of the core on that of the downcomer in the experiment. Then the most dominant frictional loss term in Eq. (51) is $\frac{1}{2} K_I |U_I| U_I$, it would be important to estimate the inlet flow resistance coefficient K_I.

The U-tube oscillation test was conducted using the test facility without heating the core. Figure 7 shows the measured and the calculated core inlet liquid velocities. The intial conditions of the test were x = 2.1 (m) and y = 0 (m). The valve between downcomer and the core was quickly opened, and the flow velocity was measured by the drag-disk flow meter.

According to Fig. 7 K_I was found to be about 30, and this value was used for all the system calculations hereafter. The resistance coefficieuts of the core and the downcomer, K_C and K_D, were temporary set to 10 and 5 respectiuely based on the conventional fricton factor correlation, however, they did not affect the result much for the current parametric study.

2. The base case calculation

The base case calculations were made to examine that the present code has a suitable feature for the system analysis. The test conditions of the base case are listed in Table 5. Since little is known about the heat transfer mechanism in

the dispersed flow region during reflood phase, the dispersed flow model of the present code was tested against the base case experiment.

Figures 8(a) and 8(b) show the effect of the dispersed flow region on the calculated boundary level elevations. The calculation without the dispersed flow region agrees with the measured quench times than that with the dispersed flow region in the upper part of the core. The switching between the two calculations were made by setting the critical Weber number from 1.0 (with dispersed flow) to 10000.0 (without dispersed flow), as it determines the critical slip velocity according to Eqs. (30)~(32), and hence the initiation of the dispersed flow boundary in the present code.

The oscillation of the boundary seen in the figures corresponds to the oscillation of the core inlet liquid velocity. Since the system under the consideration in the code is completely one-dimensional, the slight change of the mass flow rate at the core exit may cause th U-tube-type oscillation between the downcomer and the core, if the damping of the system is not large enough to prevent it.

The transition flow region, vanishing at about 250 seconds in Fig.8(a), accounts for the higher quench front velocity in Fig.8(b) after that time, as the heat transfer coefficient of the transition flow is higher than that of the dispersed flow near the quench front.

Figure 9 shows the heater rod surface temperature histories at 2.1 m elevation. Although the calculations show little pre-cooling at about 50 to 90 second, the quench time, the

quench temperature, and the overall tendency are better predicted for the case of the model without the dispersed flow region than that with it.

Figure 10 shows the same effect on the heat transfer coefficient. The calculation without the dispersed flow generally agrees well with the experiment. At the earlier stage of the transient (from 40 to 70 seconds), the measured heat transfer coefficient is much higher than the calculated one. This implies that transition flow has been established at relatively early stage in the experiment. The calculation with dispersed flow shows lower heat transfer coefficient near the quench front. This is due to the lack of the transition flow region in the vicinity of the quench front upward.

Figures 11(a) and 11(b) show the effect of the dispersed flow model on the calculated void fraction. Measured data, derived from the differential pressure measurement, are also shown in the same figures. Although the measured void fractions are smaller than the calculation in an early period (30 to 100 seconds), the calculation without the dispersed flow agrees better with the measured data than the calculation with the dispersed flow. It is considered that the flow in the experiment can better be described as a transition flow with low void fraction rather than a dispersed flow with high void fraction. Therefore we will use the code without the dispersed flow for the further calculations to assess REFLA-1D as a system analysis code.

The downcomer and core collapsed liquid levels and flooding rate are compared with the measured data in Fig.12. Except for dynamic behavior of flooding rate, calculated results

qualitatively agree with measured data. Although the collapsed liquid level of the core was predicted well, that of the downcomer was not predicted well. According to the measured and the calculated quench front elevations in Fig. 8(b), the discrepancy between the calculated and the measured downcomer liquid level is due to the slight overestimation of the vapor generation in the earlier period and to the underestimaton of it in the later period. The calculated liquid top in Fig.8(b) shows the water effluent at the core exit appears at about 120 seconds, while it was observed about 60 seconds after the reflood initiation during the experiment. This shows that the two-phase flow was established rather earlier in the experiment than the calculation. For a better prediction of the downcomer liquid level, a better prediction of the vapor flow rate at the core exit and a better two-phase flow modeling in the core would be necessary.

The input listing for the base case calculation is contained in the Apperdix.

The CPU time was about 250 seconds on FACOM M-200 for 500 seconds transient calculation.

3. Parametric calculations

3.1 Initial peak clad temperature

The calculated and the measured results on the effect of the initial peak clad temperature are shown in Fig.13. The calculated quench front elevation agrees well with the measured data. It was indicated that when the initial clad temperature is higher, the quench front moves more slowly

only in the lower portion of the core and then it moves at nearly the same velocity as that of the base case.

3.2 Peak power

The calculated and the measured results on the effect of the peak power are shown in Fig.14. The calculated quench front elevation agrees qualitatively well with the measured data. It was indicated that the higher peak power produces the smaller quench front velocity.

3.3 System pressure

Figure 15 shows the effect of the system pressure on the measured and the calculated quench front elevations. Qualitaively, the lower system pressure gave the slower quench front movement, however, the quentitative agreement between the calculation and the data was not obtained. The system pressure effect in the experiments was more significant than that in the calculation.

The measured and the calculated apparent quench temperatures at various elevations are compared in Table 6. In the case of 4 kg/cm^2a, quantitatiue agreement between the calculation and the data was obtained. Significant differences were found in the case of 1 kg/cm^2a.

Figure 16 shows the measured and the calculated collapsed liquid levels in the core and in the downcomer for the low pressure case. Nearly the same tendency as in Fig.12 is seen for the liquid levels. This shows the overall behavior of the calculated core flooding rate is nearly same as that in the experiment. Therefore, it can be considered that the large

disagreement for the low pressure case in Fig.15 comes from the weak pressure dependence of the quench velocity correlation, Eq.(34). The study of the effect of the pressure on the quench velocity correlation would be necessary for the better prediction.

V. Conclusions

1. REFLA-1D system code was developed by coupling the core thermo-hydrodynamic code and the primary system model for the system analysis of the reflood phenomena.
2. The system code without the dispersed flow model in the core was chosen for the system analysis of our small scale reflood test based on the calculation of the base case test (the base case calculation).
3. The base case calculation showed a good agreement with the data for the core collapsed liquid level, the quench front elevation, and the heat transfer coefficient near the quench front.
4. Parametric calculation showed a good agreement with the data for the effect of the initial clad temperature and of the peak power.
5. A better prediction of the vapor flow rate at the core exit and a better two-phase flow modeling in the core are necessary for a better predicion of the system behaviors.
6. The study of the quench front correlation against the dependence of the pressure is necessary for a better prediction of the quench front behaviors.

Acknowledgment

The authors are deeply indebted to Mr. T. Iguchi and Dr. Y. Sudo for their analytical support to provide thermo-hydrodynamic models for our computer codes. The authors are also very grateful to Dr. M. Nozawa and Dr. K. Hirano for hearty suggestions.

References

(1) Murao, Y.: An analytical study of the thermo-hydrodynamic behavior of the reflood-phase during a LOCA, KFK-2545, (1977).

(2) Murao, Y.: Analytical study of thermo-hydrodynamic behavior of reflood-phase during LOCA, J. Nucl. Sci. Technol., 16 [11], pp.802 ~ 817, (1979).

(3) Murao, Y. and Nagumo, H.: Examination of the reflood analysis code (REFLA-1D) by PWR-FLECHT data, JAERI-M 7382, (1977) in Japanese.

(4) Blaisdell, J.A. et al.: PWR FLECHT-SET phase A report, WCAP-8238, (1973).

(5) Murao, Y. et al: Report on series 5 reflood experiment, JAERI-M 7383, (1977).

(6) Cunningham, J.P. and Yeh, H.C.: Experiments and void correlation for PWR small-break LOCA conditions, Trans. Am, Nucl. Soc. vol. 17, 369 ~ 370 (1973).

(7) Murao, Y. and Sugimoto, J.: Correlation of heat transfer coefficient for saturated film boiling during reflood phase prior to quenching, submitted to J. Nucl. Sci. Technol.

(8) Sugimoto, J. et al.: Evaluation of heat transfer coefficients in reflood process — effect of void fraction, presented at the conference of Japan Atomic Energy society, Osaka, (1979).

(9) Kalinin E.K. et al.: Investigation of film boiling in tubes with subcooled nitrogen flow, Proc. Int. Heat Transfer Conf., 4th, Paris, (1970).

(10) Sudo, Y.: Film boiling heat transfer during reflood process in postulated PWR loss-of-coolant accident, J. Nucl. Sci. Technol., 17 [7], pp.516 ~ 530, (1980).

(11) Cermak, J.O., et al.: PWR full length emergency cooling heat transfer (FLECHT) group I test report, WCAP-7435, (1970).

(12) Groeneveld, D.C.: The thermal behaviour of a heated surface at and beyond dryout, AECL-4309, (1972).

(13) Ingebo, R.D.: Drag coefficient for droplets and solid spheres in clouds accelerating in air-streams, N.A.C.A. Techn. Note 3762 (1956).

(14) Murao, Y.: Correlation of quench phenomena for bottom flooding during loss-of-coolant accidents, J. Nucl. Sci. Technol., 15 [12], pp.875 ~ 885, (1978)

(15) Iguchi, T., et al.: Data report on series 6 reflood experiments, JAERI-M-8161, (1979). Additionally, Sudoh, T., et al., JAERI-M-8162, (1979), and Sugimoto, J., et al., JAERI-M-8169, (1979).

[Nomenclature]

A : Flow area (m^2)

Ast : Instantaneous release ratio of separated energy during quenching

C_D : Drag coefficient

C_P : Sepecific heat (kcal/kg·K)

D_d : Droplet diameter (m)

E : Emissivity (-)

G : Mass velocity ($kg \cdot h/m^3$)

G_o : Injection mass flow rate into system ($kg \cdot h/m^3$)

g : Acceleration of gravity (m/h^2)

H : Enthalpy (kcal/kg)

H_{fg} : Latent heat of evaporation (kcal/kg)

h : Heat transfer coefficient ($kcal/m^2hK$)

h_R : Radiative heat transfer coefficient ($kcal/m^2hK$)

K : Flow resistance coefficient (K-factor) (-)

L : Length (m)

L_Q : Distance from the quench front (m)

$\dot{m}$: Mass transferred from liquid plase in unit volume of two-plase mixture (kgh/m^4)

n : Number flux of droplets (l/m^2h)

p : Pressure (kg/m^2)

Q : Heat input per unit volume ($kcal/m^3h$)

Re : Reynolds number (-)

S : Cross section of flow channel (m^2)

T : Temperature (K)

t : time (h)

U : Velocity (m/h)

V : Viscous force per unit volume (kg/m^3)

V_u : Volume of upper plenum (m^3)

W_{ec} : Critical Weber number (-)

X : Set of Variables ($x, y, U_I, U_L, P_D, P_I, P_U$)

x : Liquid level of downcomer (m)

Y : Set of variables ($G_{g\ out}$, G_{out}, T_U)

y : Liquid level of core (m)

α : Void fraction (-)

ΔT_{sub} : Liquid subcooling (K)

ΔU : Slip velocity (m/h)

ε : Stefan Boltzman constant ($kcal/m^2hK^4$)

λ : Thermal conductivity (kcal/m.hK)

τ : Time constant of delayed release of stored energy after quenching

μ : Dynamic viscosity ($kg \cdot h/m^2$)

ν : Kinetic viscosity (m^2/h)

ρ : Density ($kg \cdot h^2/m^4$)

σ : Surface tension (kg/m)

Subscripts

C : Core, Cladding (in C_C), Critical (in Wec)

D : Downcomer

F : Fuel

g : Gas phase

I : Core inlet

L : Primary loop

ℓ : Liquid phase

M : Maximum

out : Core outlet

Q : Quench

R : Radiation

S : System

sat : Saturated

U : Upper plenum

W : Wall (clad surface)

Table 1 Set of correlations used in flow regions

Region	Hydro-dynamic Correlations	Heat Transfer Correlations
(1) Single Liquid Phase Flow/Subcooled Nucleate Boiling Region $Re = DeU_\ell/\nu_\ell$	$V = F \cdot 1/2 \cdot \rho_\ell / De \cdot U_\ell^2$ $F = 0.3166\ Re^{-0.25}$ $(Re \leq 2400)$ $F = 64/Re$ $(Re < 2400)$ $\alpha = 0$	$Q_\ell = L/S \cdot \phi_B$ $\phi_B = 2.197(T_w - T_{sat})^4 \cdot \exp(1.54\times10^{-6} p)$ (Jens & Lottes)
(2) Saturated Two-Phase Flow Region	$V = 0$ $\Delta U = G_g/(\alpha_{yeh} \cdot \rho_g)$, where α_{yeh} is a void fraction calculated with Cunningham-Yeh's correlation[10]. α is calculated with Eq.(17).	Same as (1). $T_\ell = T_g = T_{sat}$
(3) Subcooled Film Boiling Region	$V = 0$ $\alpha = 0$	$Q_\ell = L/S \cdot h \cdot (T_w - T_{sat})$ $h = h_{sub} + h_R$ $h_{sub} = h_{sat}(1.0 + 0.025(T_{sat} - T_\ell))$ (Sudo[7]) h_{sat} : defined in (4) $h_R = E\,\epsilon\,(T_w^4 - T_{sat}^4)/(T_w - T_{sat})$

Table 1 Continued

Region	Hydro-dynamic Correlations	Heat Transfer Correlations
(4) Transition Flow Region	Same as (2).	$Q_\ell = L/S \cdot h \cdot (T_w - T_{sat})$ $h = h_{sat} + h_R$ $h = 0.94[\lambda_g^3 \, g(\rho_\ell - \rho_g) \cdot H_{fg} \cdot g / (L_Q \mu_g (T_w - T_{sat})]^{1/4} (1-\alpha)^{1/4}$ $h_R = E(1-\alpha)^{1/2} \, (T_w^4 - T_{sat}^4)/(T_w - T_{sat})$ $T_\ell = T_g = T_{sat}$ where the physical properties of vapor are defined for the mean temperature, $T_{MEAN} = (T_w + T_{sat})/2$
(5) Dispersed Flow Region (Two-step Model) $Re = DeU_g/\nu_g$ $Re_d = D_d \Delta U/\nu_g$	$V_g = (F \text{ of } (7)) \cdot \frac{\rho_g}{De} \frac{Ug^2}{2} - V_\ell$ $V_\ell = - \frac{n}{U_\ell} \cdot C_D \cdot \frac{1}{2} \cdot \rho_g \Delta U^2 \cdot \pi \cdot \frac{Dd^2}{4}$ $\frac{n}{U_\ell} = (1-\alpha)/\{\frac{4}{3}\pi (\frac{D_d}{2})^3\}$ $C_D = \max(27 \cdot Re^{-0.84}, \, 0.4)$ (Ingebo (8))	$Q_\ell = Q_{VD} + Q_{WD}$ Wall to Vapor : $Q_{WV} = Q$ of (7) Vapor to Droplet : Q_{VD} $= \frac{n}{U_\ell} \cdot \frac{\lambda_g \pi D_d^2}{D_d} Nu_{VD} \cdot (T_g - T_{sat})$ $Nu_{VD} = 2 + 0.34 Re_d^{0.566} Pr^{1/3}$ $(Re_d \leq 1800)$ $Nu_{VD} = 2 + 0.55 Re_d^{0.5} Pr^{1/3}$ $(Re_d < 1800)$

Table 1 Continued

Region	Hydro-dynamic Correlations	Heat Transfer Correlations
(5) Dispersed Flow Region (Continued)	$We = W_{ec}$ where $W_e = \frac{\rho_g \cdot \Delta U^2 \cdot D_d}{\sigma}$ $\Delta U = \Delta U_{crit}$ α, ΔU_{crit}, Dd are calculated from eq.(17), (30) and (33) respectively.	Wall to Droplet : Q_{WD} $= \frac{L}{S} h_{RWD} \cdot (T_w - T_{sat})$ $h_{RWD} = E F_s \cdot \varepsilon (T_w^4 - T_{sat}^4)/(T_w - T_{sat})$ $F_s = \min(Sn/U_\ell \cdot \pi D_d^2/L, 1)$ $T_\ell = T_{sat}$
(6) Rewetted Flow Region	Same as (1) or (2).	Same as (1) or (2).
(7) Superheated Steam Flow Region $Re = DeU_g/\nu_g$	$V = F \cdot 1/2 \cdot \rho_f/De \cdot U_f^2$ $F = 0.3166Re^{-0.25}$ $(Re \geq 2400)$ $F = 64/Re$ $(Re < 2400)$ $\alpha = 1$	$Q_{VW} = L/S \cdot \lambda_f/De \cdot Nu(T_w - T_f)$ $Nu = 0.023Re^{0.8}Pr^{0.4}$ $(Re \geq 2400)$ (Dittus-Buelter) $Nu = \max(1.077(RePrDe/Z)^{1/3}, 3.65)$ $(Re < 2400)$

Table 2 Summary of governing equations for core

$$G_{i+1} = G_i + (\Delta Z/\Delta t)\{(\rho_\ell - \rho_{gi}(t))\alpha_i(t) - (\rho_\ell - \rho_{gi}(t-\Delta t)\alpha_i(t-\Delta t)\}$$

$$T_{\ell i+1} = T_\ell(Z - U_\ell \Delta t,\ t - \Delta t) + Q_\ell \cdot \Delta t/(\rho_\ell g C\rho_\ell)$$

$$T_{gi+1} = T_x + (T_g(Z - U_g\Delta t,\ t - \Delta t) - T_x) \cdot \exp(-A \cdot B \cdot \Delta t)$$

$$A = 1/(\alpha\rho_g \cdot g \cdot C_{pg}) \ , \quad B = (h_{wv} + h_{vD})\frac{L}{S} \ ,$$

$$T_x = \frac{h_{wv}T_w + h_{vD}T_{sat}}{h_{vw} + h_{vD}} \ , \quad h_{wv} = Q_{wv}/(T_w - T_g) \ ,$$

$$h_{vD} = Q_{vD}/(T_g - T_{sat})$$

$$\dot{m} = \{Q_\ell\}/[\{H_{fg} + C_{pg} \cdot (T_g - T_{sat})\}g]$$

$$\rho_{gi+1} = \rho_{gsat} \cdot (T_{sat} + 273.16)/(T_{gi+1} + 273.16)$$

$$G_g = U_{goi} \cdot \rho_{gi} + \Delta Z \cdot \dot{m} - \frac{\Delta Z}{\Delta t}(\alpha_i(t)\rho_{gi}(t) - \alpha_i(t-\Delta t)\rho_{gi}(t-\Delta t))$$

$$U_{goi+1} = G_g/\rho_{gi+1}$$

$$U_{\ell o} = (G_{i+1} - G_g)/\rho_\ell$$

$$\Delta U = \min(\Delta U_1,\ \Delta U^{**}_{crit}$$

where $\Delta U_1 = U_{goi+1}/\alpha^{*}_{yen}$

$$\alpha_{i+1} = \frac{1}{2}\left[1 + \frac{C1+C2}{\Delta U} - \sqrt{1 + \frac{2(C2-C1)}{\Delta U} + \left(\frac{C1+C2}{\Delta U}\right)^2}\right]$$

$$C1 = U_{goi+1} \ , \quad C2 = U_{\ell o}$$

if C2 ≤ 0 : $\alpha_{i+1} = \alpha_{yeh}$

$$DV_{i+1} = F_1 \cdot G_{gi+1}^2/(\alpha_{i+1} \cdot \rho_{gi+1}) + F_2(G_{i+1} - G_{gi+1})^2/\{(1-\alpha_{i+1})\cdot\rho_\ell\}$$

$$\left(\begin{array}{l} \alpha_{i+1} = 0 \rightarrow F_1 = 0, \quad F_2 = 1 \\ \alpha_{1+1} = 1 \rightarrow F_1 = 1, \quad F_2 = 0 \end{array}, \quad \begin{array}{l} \alpha_{i+1} \neq 0,1 \rightarrow \\ F_1 = F_2 = 1 \end{array}\right)$$

$$P_{i+1} = p_i + \Delta Z(-g\{\alpha_{i+1}\cdot\rho_g + (1-\alpha_{i+1})\rho_\ell\} - V^{***}) - (DV_{i+1} - DV_i)$$

$$U_{gi+1} = G_g/(\alpha_{i+1} \cdot \rho_\ell)$$

$$U_{\ell i+1} = (G_{i+1} - G_g)/\{(1-\alpha_{i+1}) \cdot \rho_2\}$$

Note * $\alpha_{yeh} = 0.295(\frac{\rho_{gi+1}}{\rho_\ell})^{0.239} [\frac{G_g/\rho_{gi+1}}{V_{bcr}}]^a$

where a = 0.47 $G_g/\rho_{gi+1}/V_{bcr} \leq 1$

a = 0.67 $G_g/\rho_{gi+1}/V_{bcr} < 1$

and $R_{bcr} = |\frac{1.53}{2/3}|^2 \sqrt{\frac{\sigma}{g\rho L}}$, $V_{bcr} = \frac{2}{3}\sqrt{g\ R_{bcr}}$

(Cunningham-Yeh's correlation[10])

** $\Delta U_{crit} = \min(\Delta U_2, \Delta U_3)$

where $\Delta U_2 = 0.53713\cdot(\sigma\cdot W_{ec})^{0.3801} \rho_g^{-0.5868}$

$$\nu_g^{-0.1736} \cdot (\rho_\ell \cdot g)^{0.2066}$$

$$\Delta U_3 = 1.3512 \cdot (\frac{\rho_\ell \cdot g \cdot \sigma \cdot W_{ec}}{\rho_g^2})^{0.25}$$

$$Dd = \frac{W_{ec}\cdot\sigma}{\rho_g \cdot \Delta U_{crit}^2}$$

*** See Table 1

Table 3 Main specification of small scale reflood test facility

Bundle geometry	
Arrangement	4 × 4 - rod (square pitch)
Outer diameter of rod	10.5×10^{-3} m
Pitch	13.8×10^{-3} m
Heated length	3.6 m
Housing dimension	60×10^{-3} m square
Heater rod design	
Type	Indirect heating type
Clad thickness	1.3×10^{-3} m
Clad material	Inconel 600
Heating element outer diameter	6.4×10^{-3} m
Heating element material	Nichrome
Attached thermo-couple	0.5×10^{-3} m o.d. ungrounded type

Table 4 Parametric range of test conditions

System Pressure	1 ~ 4 ata
Peak Power	1.6 ~ 2.4 KW/m
Supplied Water Velocity into Downcomer	4 ~ 8 cm/sec
Initial Peak Clad Temperature	550 ~ 700 °C
Supplied Water Temperature	80 ~ 120 °C
Core Housing Temperature	100 ~ 140 °C

Table 5 Test condition of base case

System Pressure	2 ata
Peak Power	1.6 leW/m
Supplied Water Velocity	4 cm/sec
Initial Peak Clad Temperature	550 °C
Inlet Subcooling	20 °C
Core Housing Temperature	120 °C

Table 6 Summary of measured and calculated quench temperatures

Elevation (m)		0.325	0.8	1.3	1.5	1.8	2.1	2.3	2.55	2.9	3.275
Base Case	Calculated	229	377	440	517	511	534	470	501	423	331
	Measured		319	365	464		450		383	345	
						503	413	408		329	
			339	323	451		407		392	294	
1ata	Calculated	229	381	458	558	562	609	-	-	-	
	Measured		279	333	462		451		430	367	
						512	448	415		338	
			318	315	456		422		416	318	
4ata	Calculated	226	381	437	503	490	498	437	-	-	
	Measured		370	383	579		483		394	365	
						512	448	434	385		
			349	364	479		445		351	352	

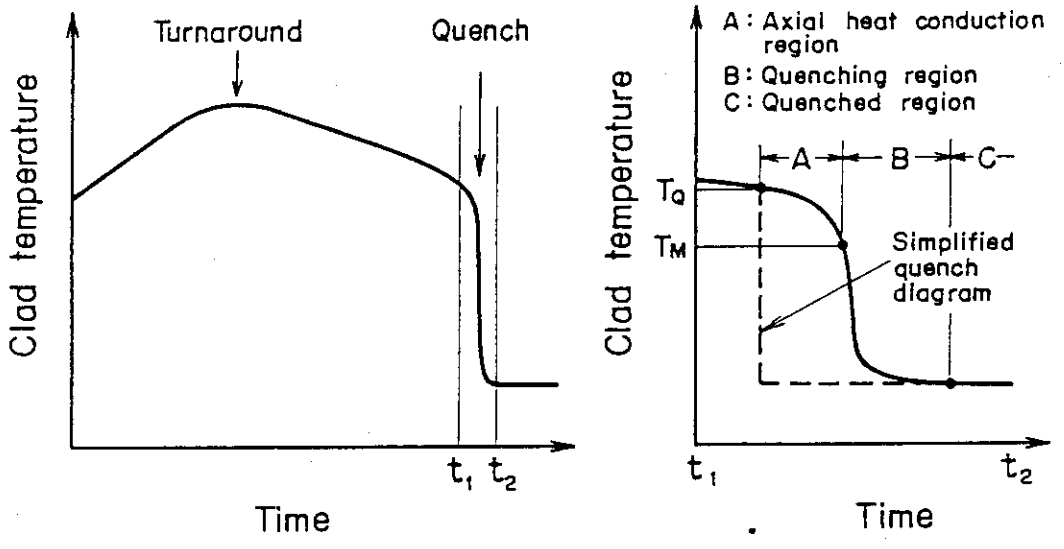

(a) Temperature-time history during reflood phase

(b) Detail of temperature-time history in quenching period

Fig. 1 Schematic diagram of temperature-time history during reflood phase

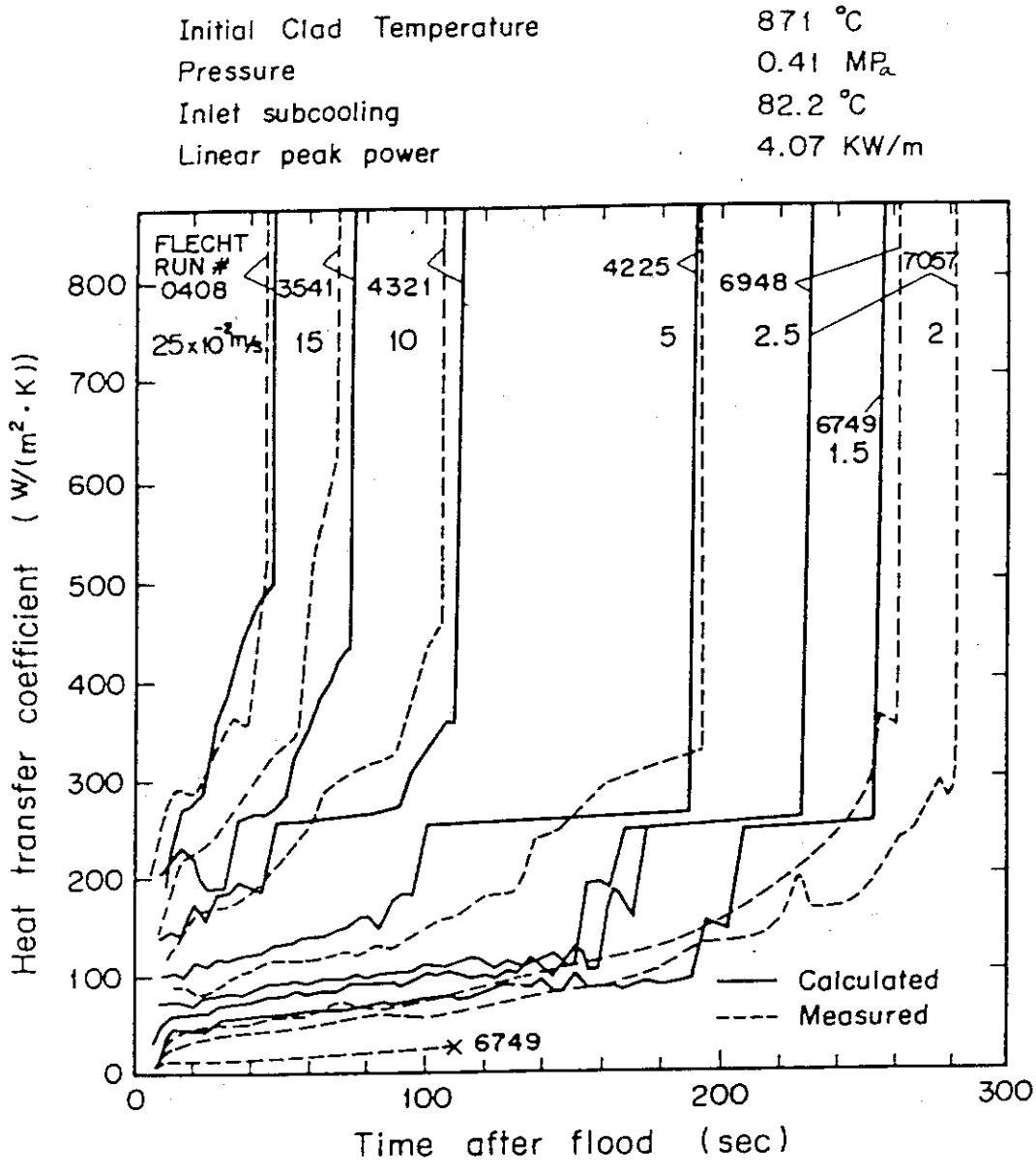

Fig. 2 Comparison of measured heat transfer coefficients with those calculated with original REFLA – 1D

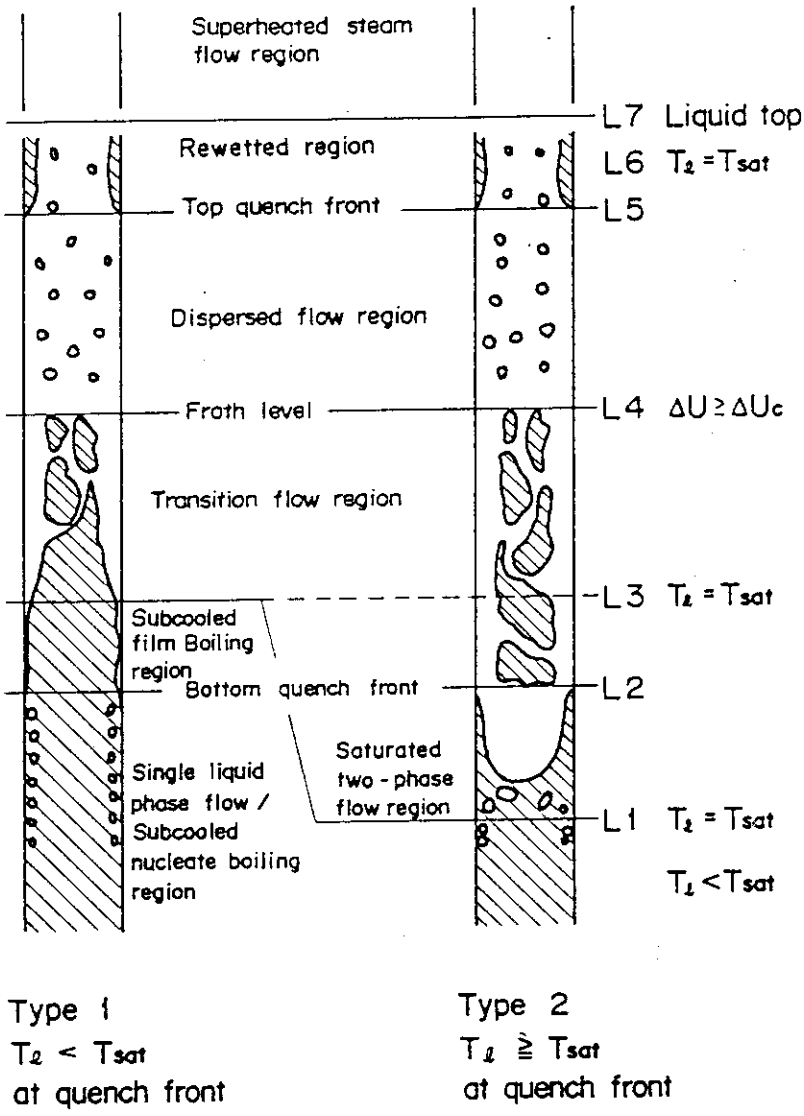

Fig. 3 Reflood flow model and definition of boundaries

T_ℓ : Liquid Temperature
T_{sat} : Saturation Temperature
ΔU : Slip velocity between two-phases
ΔU_c : Critical slip velocity

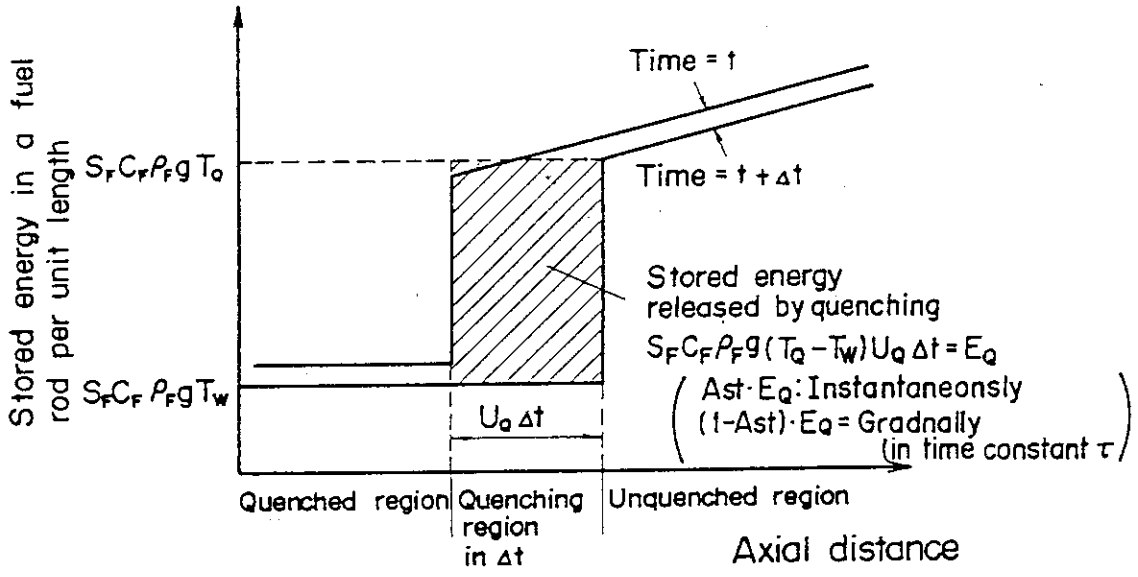

Fig. 4 Release of stored energy from a fuel rod during quenching
(Heat capacity of a fuel rod per unit length $= S_F C_F \rho_F g$)

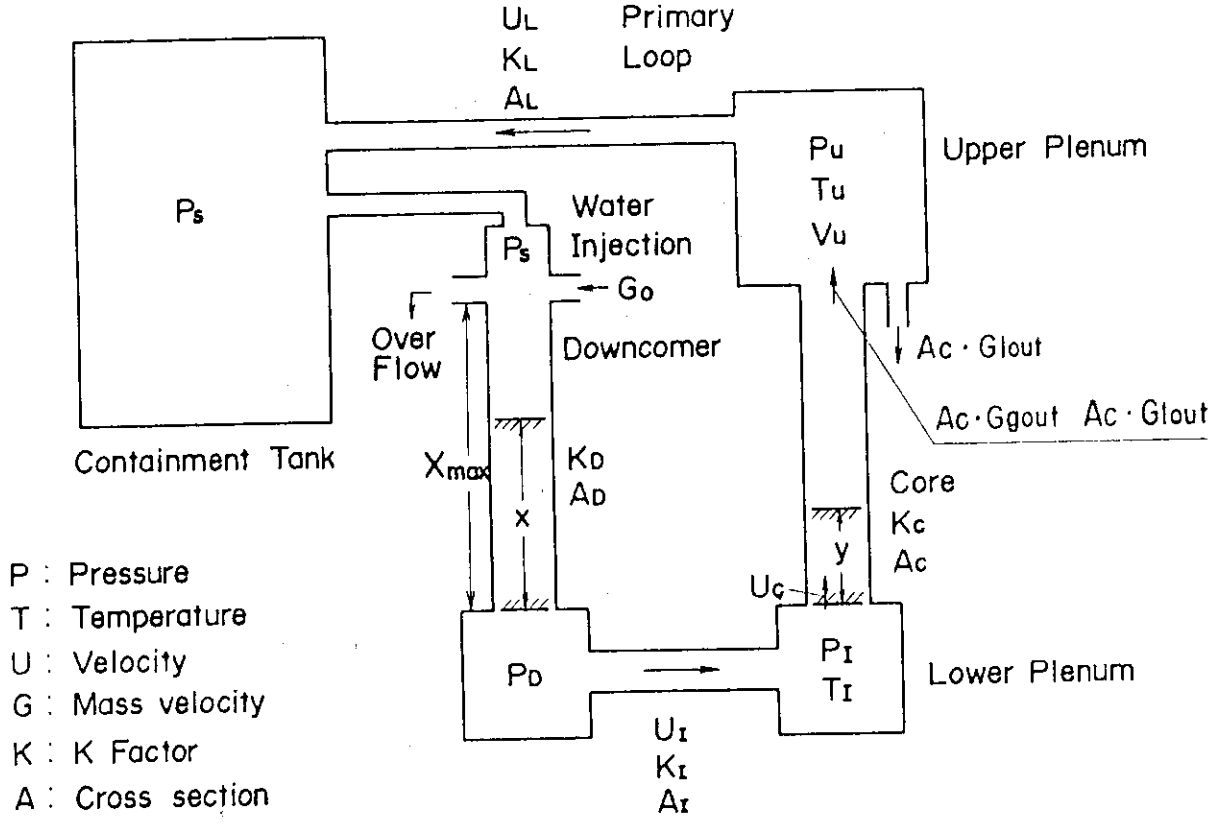

Fig. 5 Schematic diagram of system code model

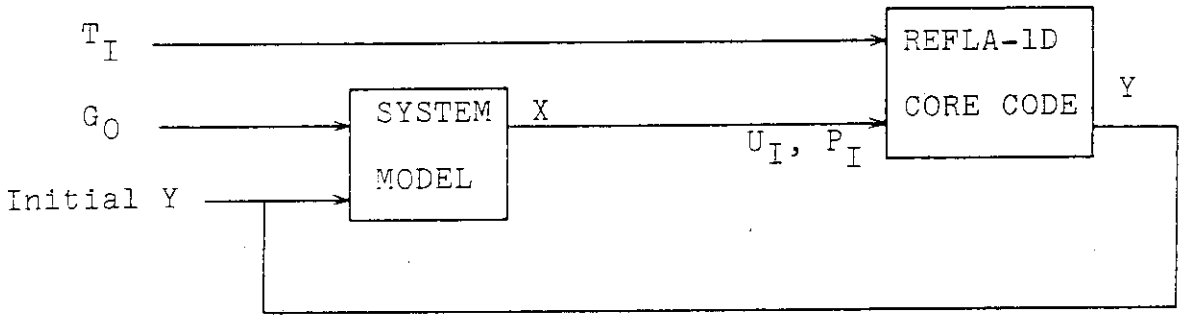

Fig. 6 System calculation procedure

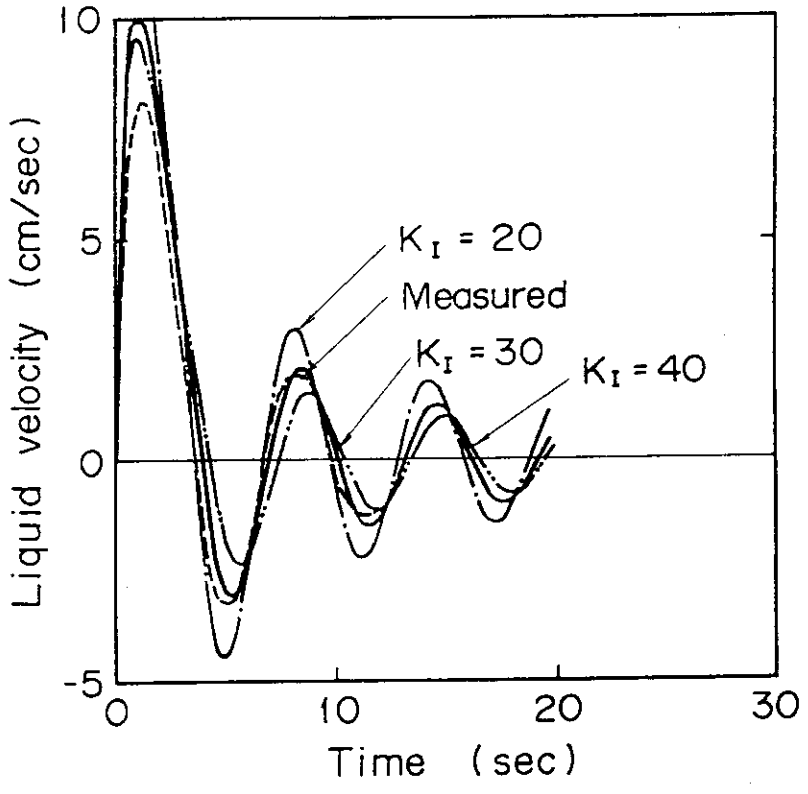

Fig. 7 Measured and calculated core inlet flow velocity

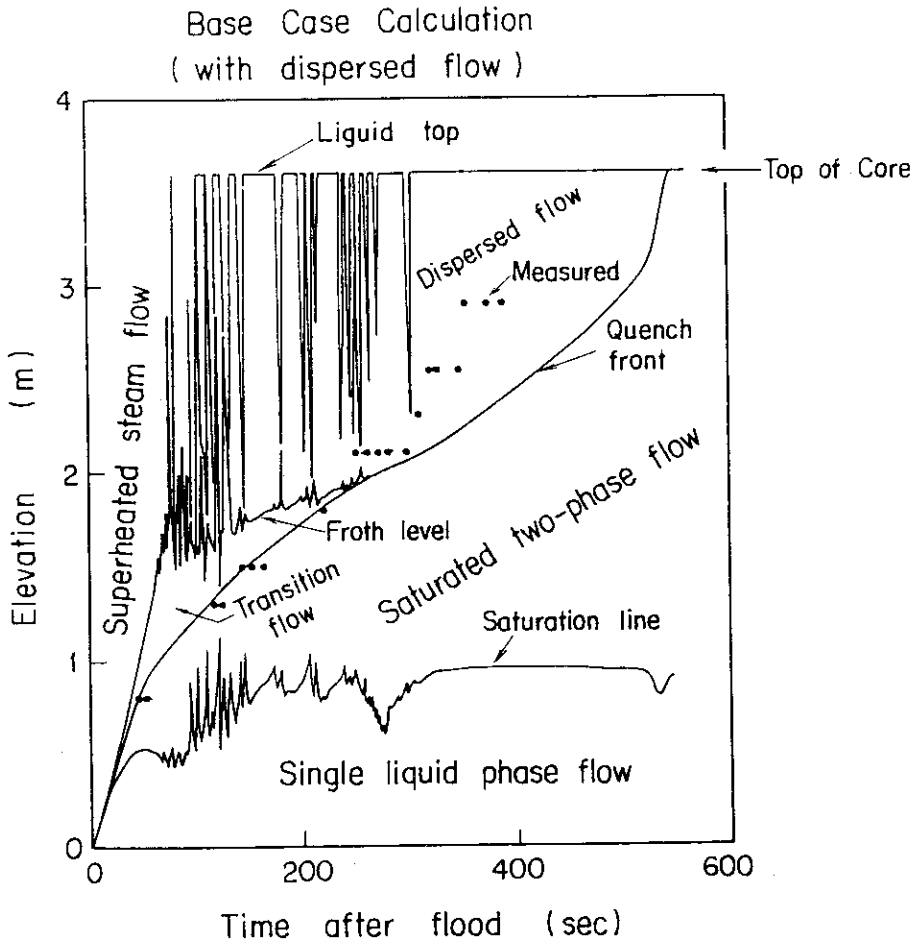

Fig. 8(a) Boundary levels calculated by REFLA-1D with the dispersed flow region and the measured quench times

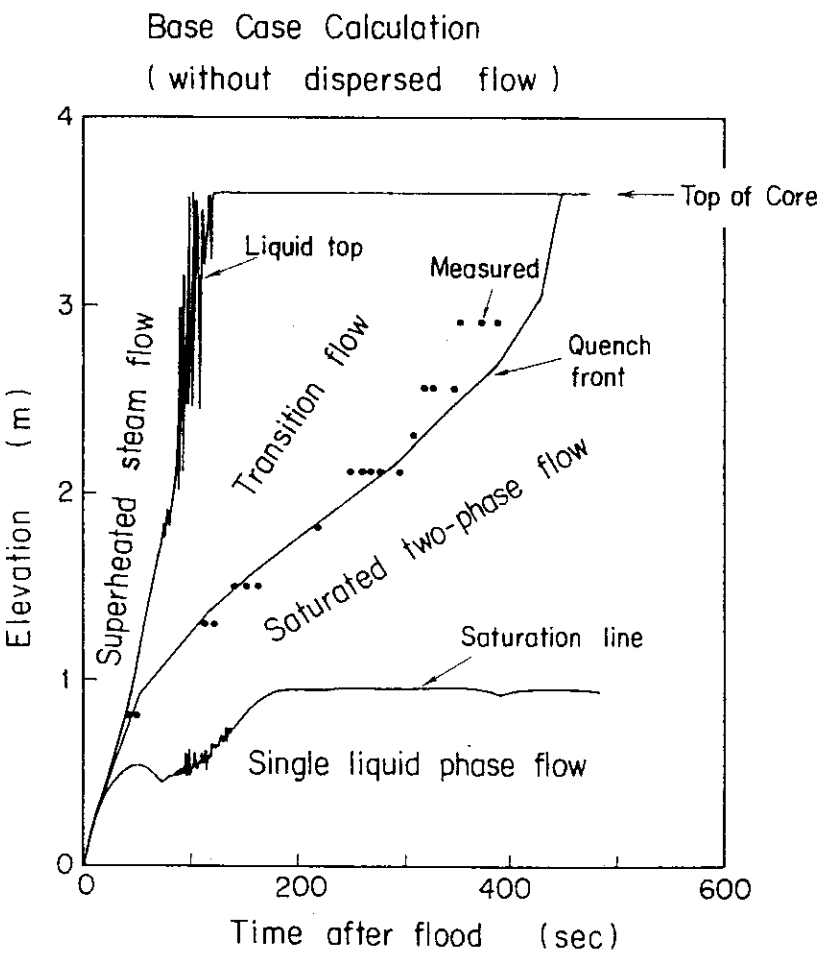

Fig. 8(b) Boundary levels calculated by REFLA-1D without the dispersed flow region and the measured quench times

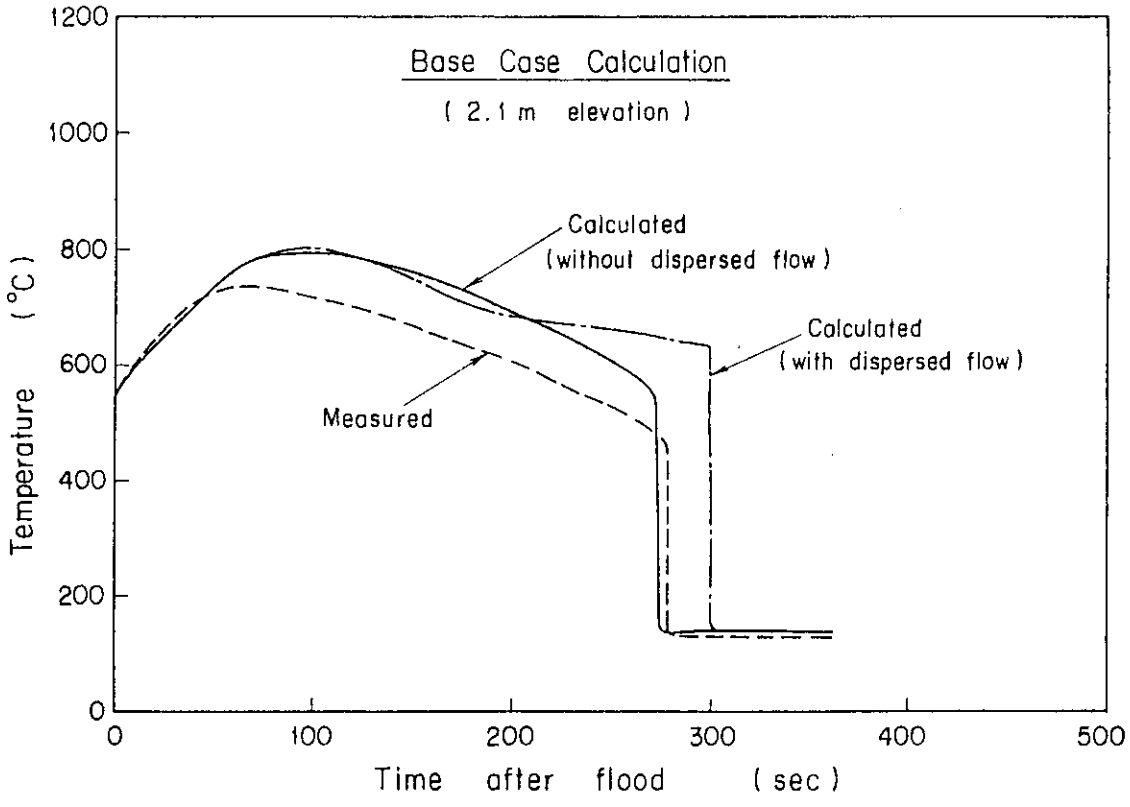

Fig. 9 Effect of the dispersed flow region on the calculated heated rod surface temperature

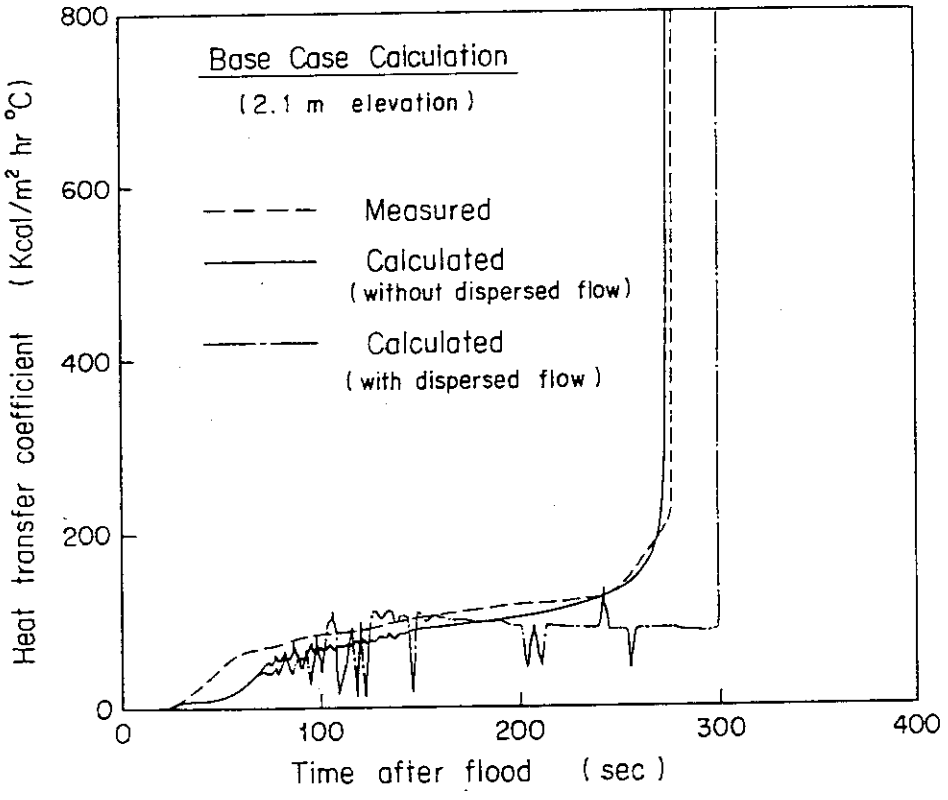

Fig. 10 Effect of the dispersed flow region on the calculated heat transfer coefficient

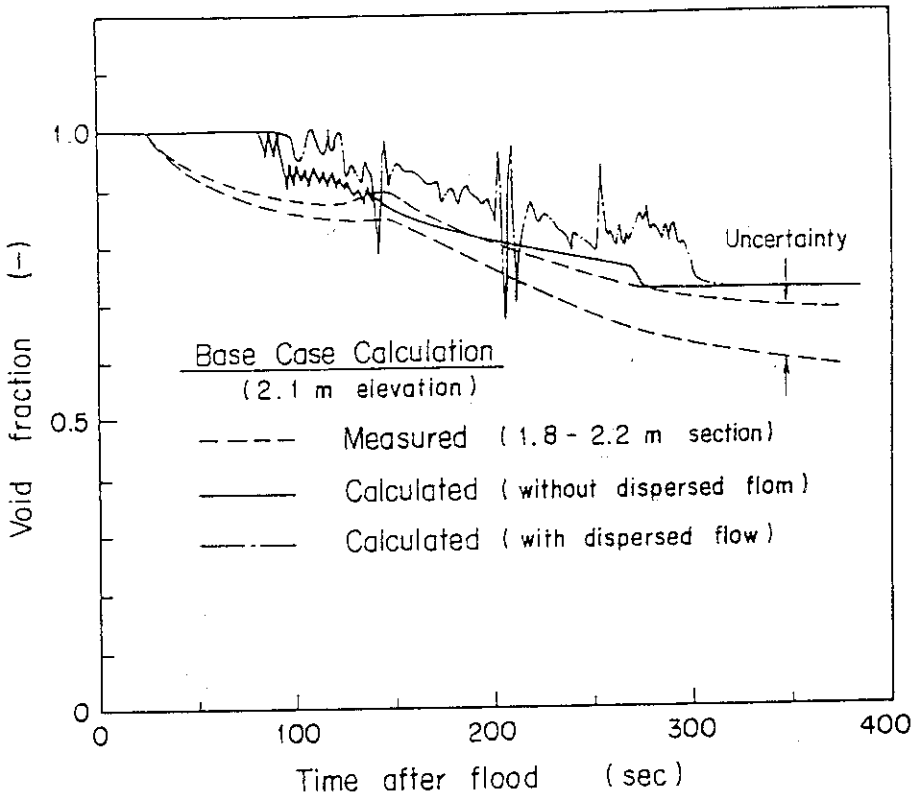

Fig. 11 (a) Effect of the dispersed flow region on the calculated void fraction

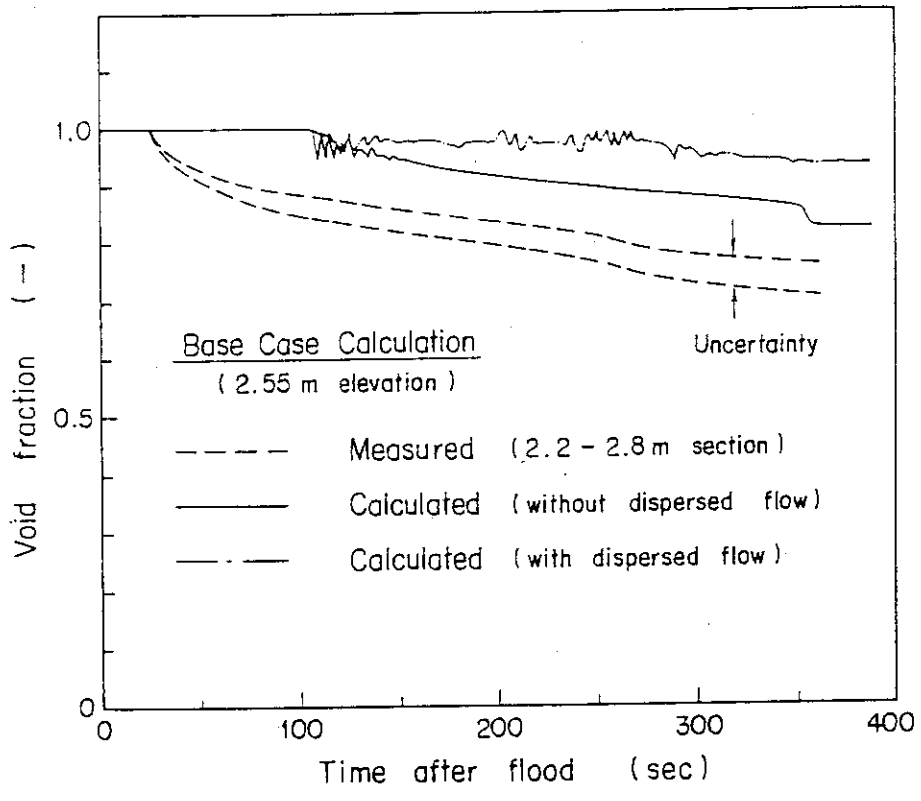

Fig. 11 (b) Effect of the dispersed flow region on the calculated void fraction

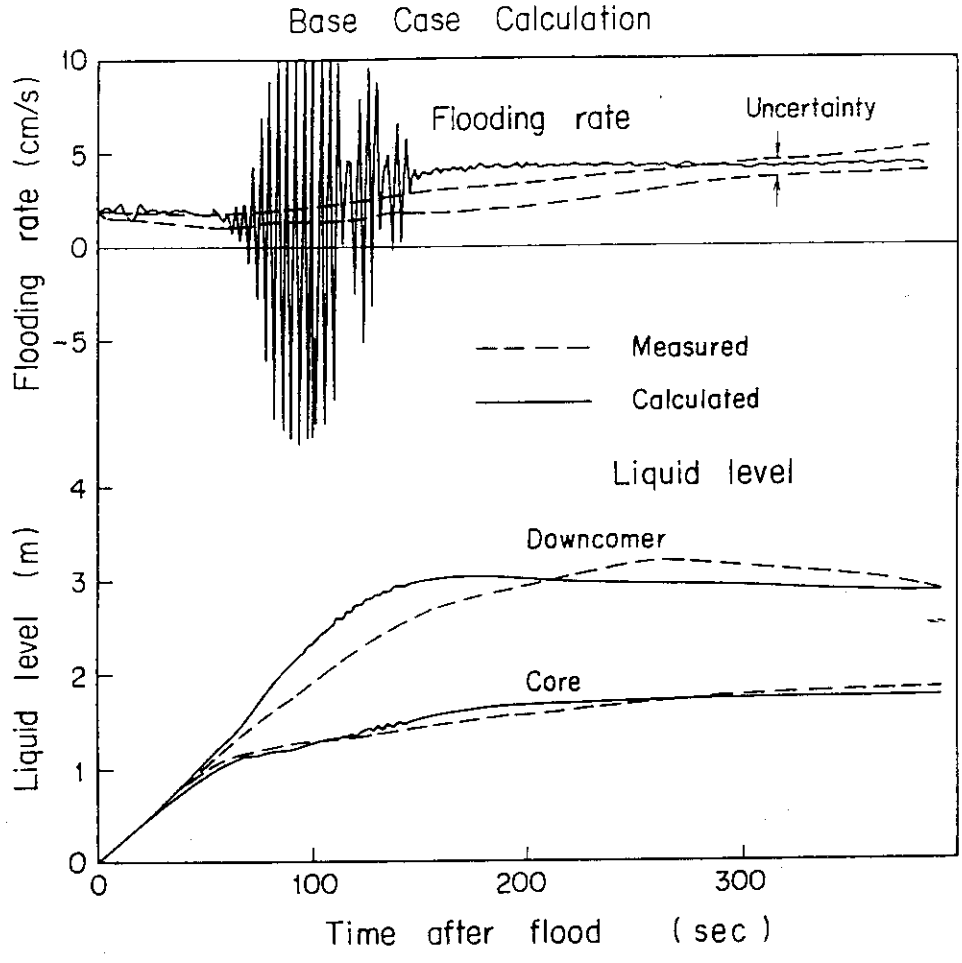

Fig.12 Comparion of measured and calculated results on downcomer and core collapsed liquid level and flooding rate

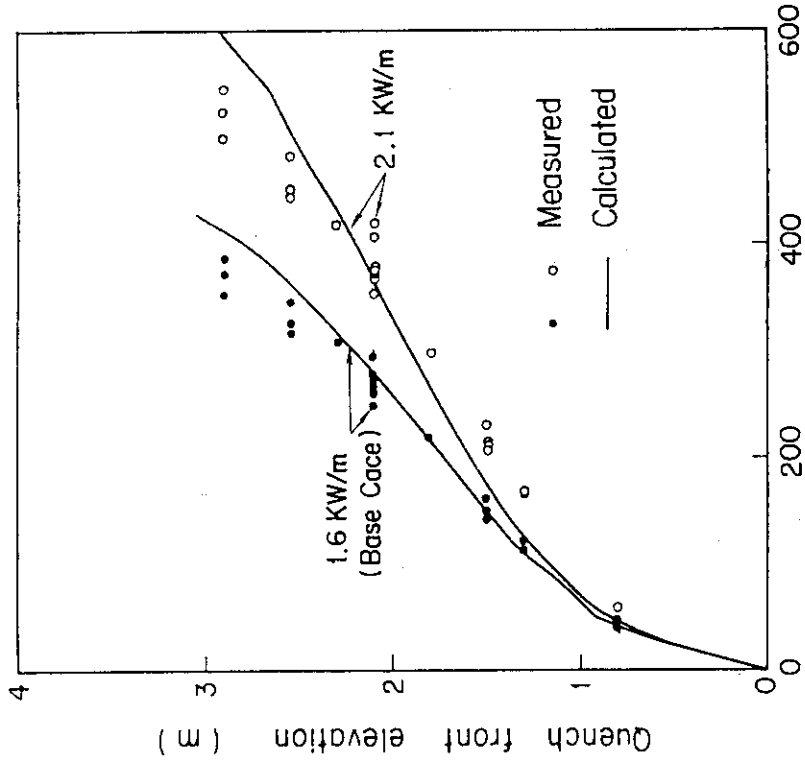

Fig. 14 Effect of the peak power on the measured and the calculated quench front elevations

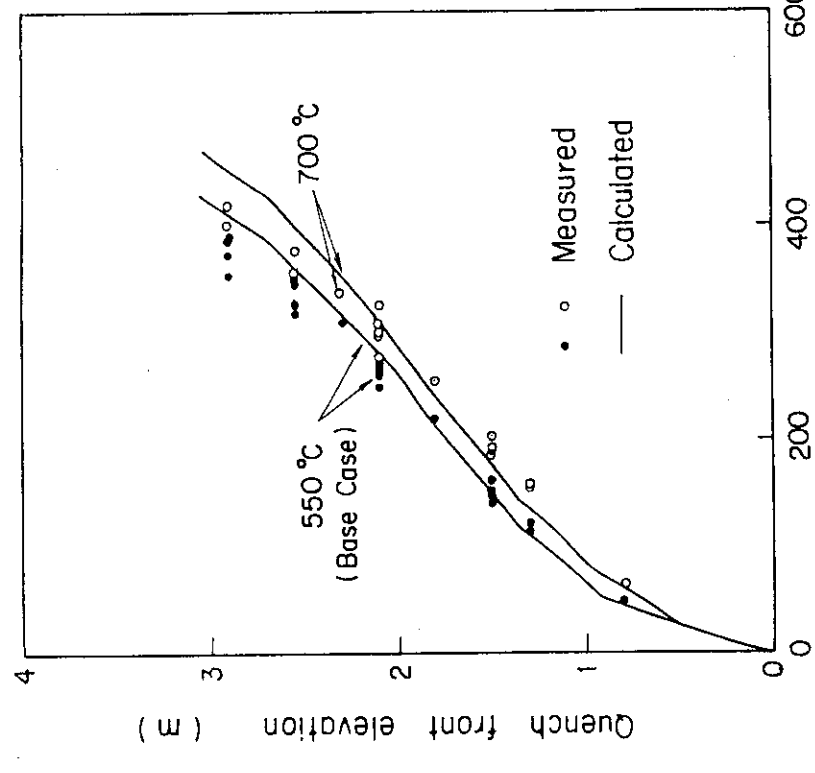

Fig. 13 Effect of the initial peak clad temperature on the measured and the calculated quench front elevations

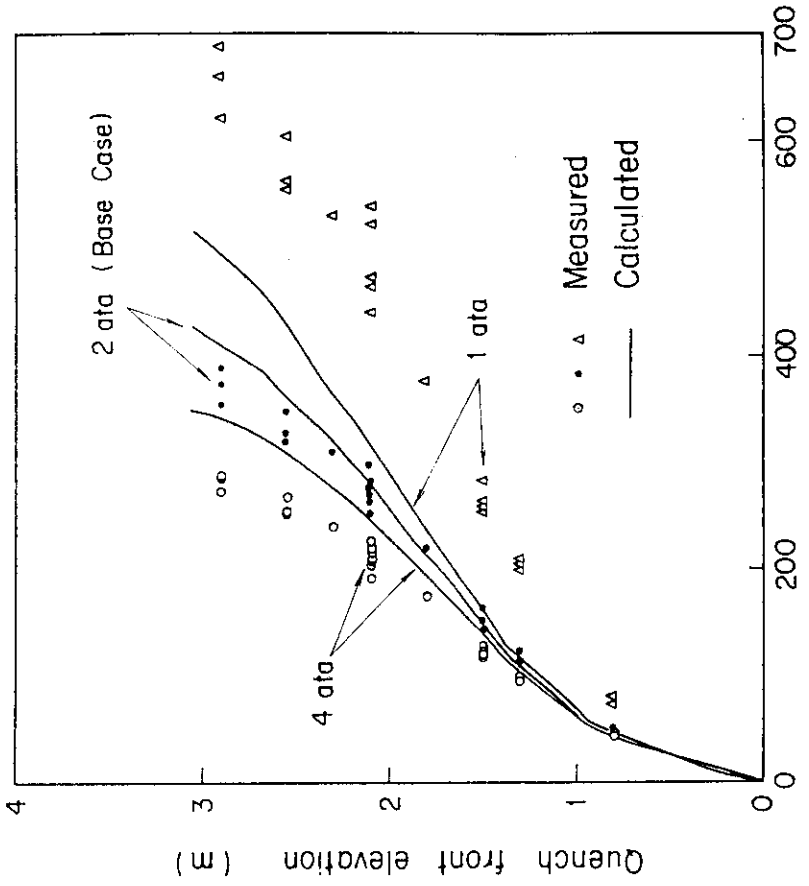

Fig. 15 Effect of the system pressure on the measured and the calculated quench front elevations

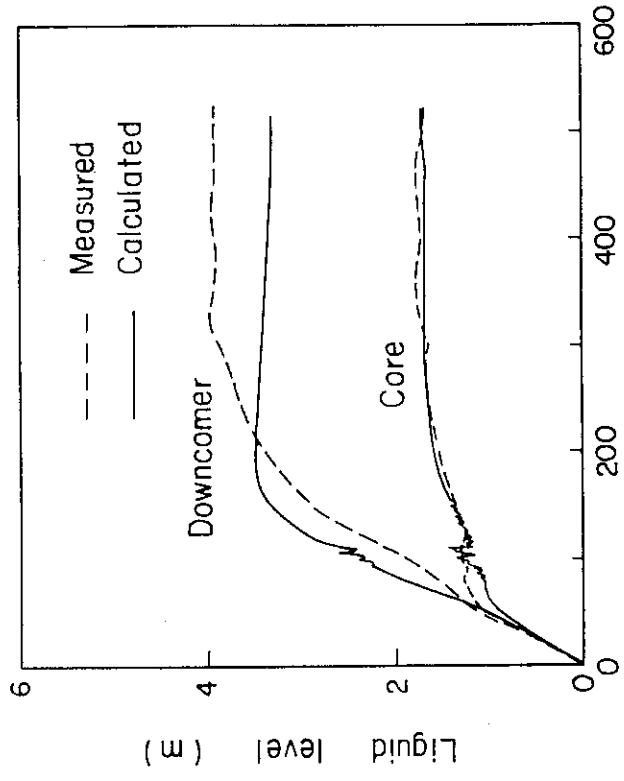

Fig. 16 Comparison of measured and calculated collapsed liquid level for 1 ata system pressure

* * * * INPUT CARDS LIST * * * *

```
NO.       .....1.....2.....3.....4.....5.....6.....7.....8.....9....10....11....12....13..

  1      (TEST CALCULATION OF RUN 6512  WITH WEC = 10000.0                          00000010)
  2      (       1.600         0.10          4.0         100.         2.000        2.00000000020)
  3      (       100.0        4.200         4.20         0.005                     2.0  00000030)
  4      (         500                                                             00000040)
  5      (          90                       10.5          13.8          3.6          400000050)

  6      (     10000.0           1.0          0.10          2.00          0.0          1.000000060)
  7      (                                    10.8        2000.0       0.41318         00000070)
  8      (           2                                                               00000080)
  9      (                     140.0         4.068                      1.429        83.8900000090)
 10      (        20.0         550.0         4.068          2.54                      00000100)

 11      (       500.0                                      2.54                      00000110)
 12      (       500.0                                                                00000120)
 13      (       500.0        1200.0                                                  00000130)
 14      ( 210.0 210.0 210.0 210.0 210.0 210.0 210.0 210.0 210.0 210.0 210.0 210.000000140)
 15      ( 210.0 323.0 323.0 323.0 323.0 323.0 323.0 323.0 323.0 323.0 323.0 323.000000150)

 16      ( 427.0 427.0 427.0 427.0 427.0 427.0 427.0 427.0 427.0 427.0 427.0 550.000000160)
 17      ( 550.0 550.0 550.0 550.0 550.0 550.0 550.0 550.0 550.0 550.0 550.0 550.000000170)
 18      ( 550.0 550.0 550.0 550.0 550.0 550.0 550.0 425.0 425.0 425.0 425.0 425.000000180)
 19      ( 425.0 425.0 425.0 425.0 425.0 425.0 425.0 318.0 318.0 318.0 318.0 318.000000190)
 20      ( 318.0 318.0 318.0 318.0 318.0 220.0 220.0 220.0 220.0 220.0 220.0 220.000000200)

NO.       .....1.....2.....3.....4.....5.....6.....7.....8.....9....10....11....12....13..

 21      ( 220.0 220.0 220.0 220.0 220.0 220.0 220.0                                00000210)
```